Adsorption of Natural Organic Matter to Air–Water Interfaces during Transport through Unsaturated Porous Media

ARTICLE *in* ENVIRONMENTAL SCIENCE AND TECHNOLOGY · FEBRUARY 2004

Impact Factor: 5.33 · DOI: 10.1021/es034409a · Source: PubMed

2 AUTHORS, INCLUDING:

John J Lenhart
The Ohio State University
35 PUBLICATIONS **1,605** CITATIONS

Environ. Sci. Technol. **2004**, *38,* 120−126

Adsorption of Natural Organic Matter to Air−Water Interfaces during Transport through Unsaturated Porous Media

JOHN J. LENHART† AND JAMES E. SAIERS*

School of Forestry and Environmental Studies, Yale University, 205 Prospect Street, New Haven, Connecticut 06511

To better understand how interactions with the air phase influence the movement of natural organic matter (NOM) through the vadose zone, we measured the transport of soil−humic acid (SHA) through laboratory columns packed with partially saturated sand. Our results demonstrate that sorptive reactions at air−water interfaces reduce SHA mobility and that the affinity of SHA for the air phase increases as the porewater pH declines from 8 to 3.9. SHA desorption from air−water interfaces is negligible for conditions of constant pH, but release of bound SHA occurs in response to perturbations in porewater pH. We analyzed the effluent samples collected from our laboratory columns using high-performance size-exclusion chromatography. The results of this analysis demonstrate that the SHA did not fractionate appreciably during transport through the columns, suggesting that the various components of the SHA pool (as distinguished on the basis of molecular weight) express an equal affinity for the air−water interfaces over the range of pH conditions tested. A mathematical model incorporating irreversible, second-order rate laws to simulate adsorption at air−water and solid−water interfaces closely describes the SHA breakthrough data. The mass-transfer parameters that govern this model vary in a discernible fashion with changes in porewater pH, and the parameter trends are consistent with published theories for SHA adsorption.

Introduction

Natural organic matter (NOM) consists of a mixture of polyfunctional molecules of varying size and reactivity. NOM is ubiquitous in soil−water systems and binds organic and inorganic contaminants; therefore, the transport of NOM may, under some circumstances, govern the fate and distribution of contaminants in the vadose zone (*1*). The presence of hydrophilic (e.g., carboxylic, phenolic, and other oxygen-containing groups) and hydrophobic functional groups (e.g., aromatic rings, fatty acid esters, and aliphatic hydrocarbons) contributes to the high surface reactivity of NOM macromolecules, and like other surface-active materials, NOM partitions to solid−water and air−water interfaces (*2*, *3*). Quantification of these interfacial reactions is critical to prediction of the migration of NOM and NOM-associated contaminants through soil−water systems.

Humic acids (HA) and fulvic acids (FA) account for 40−60% of the organic carbon in NOM of terrestrial origin (*4*, *5*). Much of the physicochemical behavior of these substances reflects the presence of 1.5−11.2 mmol/g carboxylic and 0.3−6.0 mmol/g phenolic functional groups (*6*). The acidity of FA is generally greater than the acidity of HA, but the dissociable proton content of both substances exceeds that of other soil constituents (e.g., clays) (*6*, *7*). Only the strongest acidic groups of NOM deprotonate at low pH (i.e., pH < 3), so under these conditions, polarity and solubility are low (*4*) and retention at interfaces is high (*8*−*10*). Increasing solution pH promotes functional-group dissociation, which increases the hydrophilic and polar nature of NOM and reduces sorption at mineral surfaces and retention at air−water interfaces (*8*, *10*).

NOM exhibits a distribution in sorptive characteristics due to heterogeneity in the size and composition of its components. Although exceptions exist, the affinity for mineral surfaces and air−water interfaces is generally greater for larger, more hydrophobic components than for smaller, more hydrophilic components (*3*, *11*−*14*). This nonuniformity in sorptive characteristics may promote fractionation of NOM during transport, as weakly sorbing fractions move through the porous medium at greater apparent velocities than strongly sorbing fractions (*15*−*17*). Because different components of the NOM pool express varying capacities to bind dissolved chemicals, fractionation of NOM by molecular weight or by composition has important implications to contaminant fluxes through the vadose zone (*16*, *18*).

Studies on NOM transport through water-saturated soils demonstrate that sorption at solid−water interfaces is sensitive to solution chemistry, NOM concentration, and mineral−grain composition (*17*, *19*); however, comparatively little attention has been devoted to evaluating the response of NOM adsorption at air−water interfaces to changes in the properties of the soil−water system. Consequently, it is impossible to infer how NOM moves through the vadose zone, where both air and water occupy the pore spaces. The overall goal of the work reported here is to advance our understanding of the role of air−water interface reactions in the transport of NOM through water-unsaturated porous media. We examined the transport of soil−humic acid (SHA) through saturated and unsaturated sand columns in a series of experiments distinguished on the basis of porewater pH. The sand used in these experiments was chemically treated to minimize sorptive reactions at the solid−water interfaces, thereby enabling air-phase influences on SHA mass transfer to be isolated. We evaluated SHA fractionation during transport by comparing the molecular weight distribution and polydispersity of the influent and effluent samples, and we applied a simple transport model to the SHA breakthrough data to quantify how the rates of SHA adsorption at air−water interfaces respond to changes in porewater pH. The results of this research reveal that sorptive reactions at air−water interfaces produce measurable effects on porewater concentrations of SHA and suggest that accounting for these air-phase reactions in transport models is requisite to accurate simulation of NOM movement through the vadose zone.

Experimental Methods

Preparation of Materials. Quartz sand was used as the porous medium (Accusand 40/60, Unimin Corp.) in both the

* Corresponding author phone: (203)432-5121; fax: (203)432-5023; e-mail: james.saiers@yale.edu.

† Present address: Department of Civil and Environmental Engineering and Geodetic Science, The Ohio State University, Columbus, OH 43210.

10.1021/es034409a CCC: $27.50
Published on Web 11/14/2003

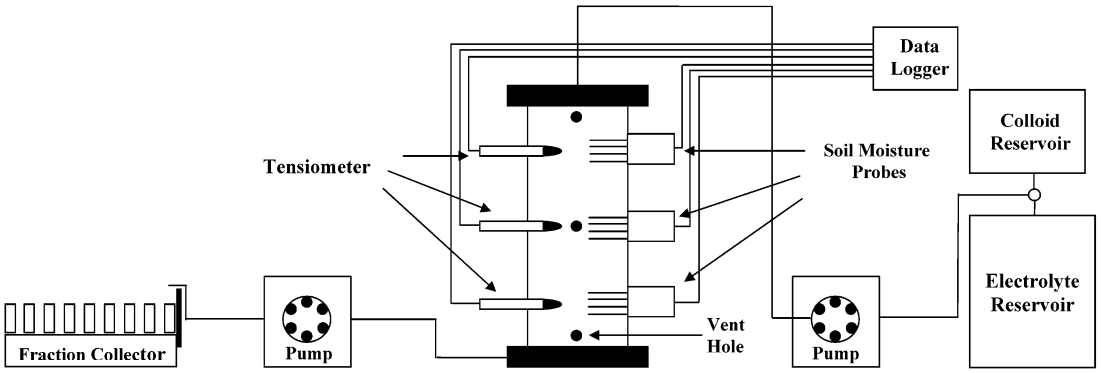

FIGURE 1. Schematic of the laboratory columns used in the experiments on SHA transport.

saturated and unsaturated experiments. The fraction of sand between 300 and 355 μm was isolated for use with stainless steel sieves and a sieve shaker (RX-29 Ro-Tap, W. S. Tyler). As received from the distributor, the surfaces of the sand grains were coated with oxides of Al, Fe, and Ti and trace amounts of organics. We removed these coatings from the sieved-sand fraction through a sequence of acid and base washes, as outlined by Lenhart and Saiers (*20*).

An Elliott SHA standard, purchased from the International Humic Substances Society, served as the NOM in the experiments. Compared with NOM isolated from other freshwater systems (e.g., rivers), soil humic acids have a high molecular weight and carbon content, but low oxygen content, carboxyl content, and total acidity (*21*−*23*). We prepared a 500 mg/L SHA solution with deionized water for each column experiment. After adjusting the pH to 7 with NaOH, the stock solution was equilibrated overnight to ensure complete dissolution of the SHA. SHA solutions (20 mg/L) applied to the columns were made by diluting the 500 mg/L stock with 0.01 M NaCl and by adjusting the pH of this solution (with NaOH or HCl) to 3.9, 5.0, 7.3, or 8.0. In preliminary experiments, we verified that the SHA remained completely dissolved following pH adjustment.

Column Design. Lenhart and Saiers (*20*) provide a detailed description of the column construction and instrumentation, which we summarize here. For each experiment, fresh sand was wet-packed into acrylic columns measuring 12.7 cm in diameter and 32.8 cm in length (Figure 1). The porosity of the sand bed equaled 0.335. Probes for measuring the volumetric moisture content (ML2x Thetaprobe, Delta-T Devices, Ltd.) and tensiometers [consisting of ceramic cups (2100-200CR-B1M3, Soil Moisture, Corp) connected to differential microtransducers (26PCAFA6D, Honeywell/Microswitch)] for monitoring capillary pressure head were located at 7.7, 16.4, and 25.1 cm from the top of the column. Data from the moisture probes and tensiometers were collected using a datalogger (DL2e, Delta-T Devices, Ltd.). Peristaltic pumps (Cole-Parmer Instrument Co) at the inflow end (top) and outflow end (bottom) of the column regulated the downward flow of water in the experiments with unsaturated sand; one peristaltic pump, located at the outflow end, controlled the flow of water in experiments with saturated sand.

Unsaturated Column Experiments. We conducted experiments in unsaturated media at four porewater pH values: 3.9, 5, 7.3, and 8. Preparation for each experiment involved draining the sand pack (which was initially saturated with a pH-adjusted 0.01 M electrolyte solution) by elevating the outflow rate 3 cm^3/min above the inflow rate. Approximately 5 h was required to drain each column to a spatially uniform moisture content (Θ) and capillary pressure head (Ψ) of 0.120 $\pm$ 0.004 and -29.8 ± 0.5 cm, respectively. Upon reaching the target Θ, a unit hydraulic-head gradient throughout the sand pack was established by setting the outflow rate equal to the inflow rate. The average linear porewater velocity under steady and uniform flow equaled 0.66 cm min^{-1}. Once the effluent pH matched the influent pH, a 20 mg/L SHA solution (prepared as described above) was introduced to the top of the column as a 3.5-L pulse. This pulse was followed by a SHA-free electrolyte solution (at the same pH), which was applied until effluent concentrations of SHA returned to baseline levels. Water samples were collected throughout the experiments from the base of the column in glass test tubes with a fraction collector (IS-95, Spectrum Chromatography Inc.). Humic acid concentrations in the water samples were determined by two techniques: (i) measuring the UV absorbance at a wavelength of 254 nm with a UV−visible spectrophotometer (DU 520, Beckman) and (ii) measuring the total organic carbon content with a TOC analyzer (TOC-5000, Shimadzu). Sample UV absorbance was converted to SHA concentration based upon calibration to standard samples containing unaltered SHA. TOC measurements were calibrated using standards prepared from a 1000 mg/L reference solution (AccuStandard Inc.). Both methods yielded virtually identical sample concentrations. So, except for one pair of TOC and absorbance data for the saturated experiments (Figure 2B) and unsaturated experiments (Figure 3C), we report only the measurements made with the spectrophotometer.

At the conclusion of the experiment at pH 3.9, we induced desorption of SHA retained within the column by increasing the pH of the influent solution in two steps. A pH 5 solution was applied in the first step for 2.3 pore volumes, and a pH 7.3 solution was applied for 14.3 pore volumes in the second step. Samples were collected as described previously and analyzed for pH and SHA concentration.

Saturated Column Experiments. Experiments in the saturated media were conducted at pH 3.9, 5, and 7.3 in a similar fashion as the unsaturated experiments, except the initial step of sand-pack draining was omitted. The SHA influent concentration (20 mg/L), background electrolyte (0.01 M NaCl), and average linear porewater velocity (0.66 cm min^{-1}) were the same for both types of experiments. We found that SHA retention within the water-saturated sand columns decreased as the pH increased. Because SHA transport through the saturated media was nonreactive at pH 7.3, the experiment at pH 8 was deemed unnecessary.

Size-Exclusion Chromatography. The number and weight average molecular weights of SHA in influent and effluent samples were determined using high-performance size-exclusion chromatography (HPSEC) according to the procedure outlined by Zhou et al. (*24*). Our HPSEC system consisted of an HPLC pump (GP 40, Dionex Corp.), a variable-wavelength absorbance detector (AD20, Dionex Corp), and an automated six-position injection valve (9126-042, Rheodyne, L.P.) equipped with a 20-μL sample loop. We used a modified silica column (Protein Pack 125A, Waters Associates) and a mobile phase consisting of 0.1 N NaCl, buffered to

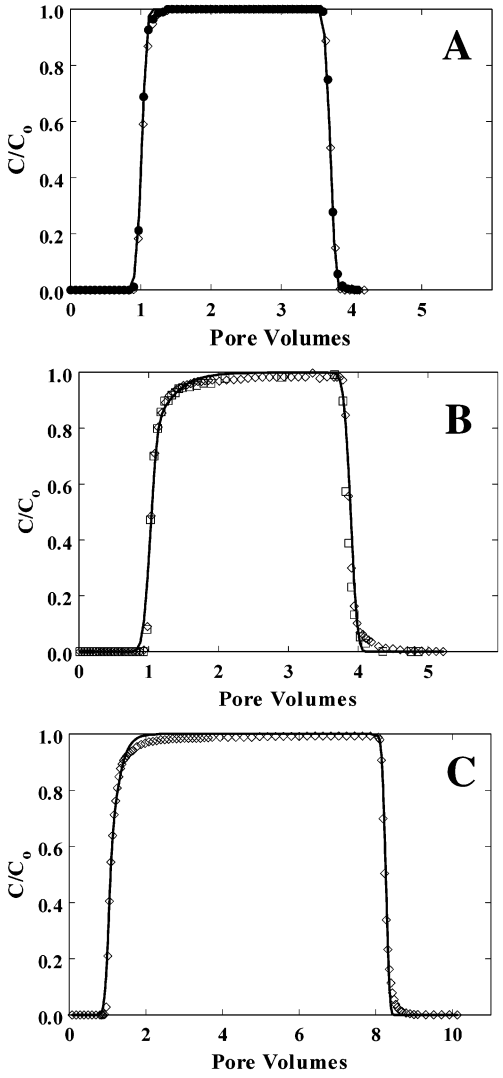

FIGURE 2. Measured breakthrough curves for the transport of SHA (open diamonds and open squares) and bromide (closed circles) in water-saturated media at a pH of (A) 7.3, (B) 5, and (C) 3.9. The solid line in panel A represents a model simulation for nonreactive solute transport, whereas the solid lines in panels B and C delineate model concentrations calculated assuming rate-limited adsorption at solid−water interfaces (see eqs 3 and 4). SHA concentrations determined using the UV−vis spectrophotometer (open diamonds) were nearly equal to those measured using the TOC analyzer (open squares), thus TOC measurements are only shown in panel B. A pore volume equals $qt/L\Theta$, where L is the column length.

pH 6.8 with phosphate (0.002 M Na_2HPO_4 and 0.002 M NaH_2PO_4). Prior to analysis, the pH and ionic strength of the humic acid samples were adjusted to 6.8 and 0.1 M, respectively. Standard and experimental samples were delivered to the column at a flow rate of 1.0 mL/min and detected at a wavelength of 230 nm. Following the recommendations of Zhou et al. (*24*), the elution time was converted to molecular weight using 100 mg/L polystyrene sulfonate (PSS) (35, 18, 8, and 4.6 kDa, Polysciences Inc.), 100 mg/L salicylic acid, and 5% acetone solutions. The weight average molecular weight (M_w), number average molecular weight (M_n), and polydispersity (M_w/M_n) of sample chromatograms were calculated assuming constant sample absorptivity with the following equations:

$$M_n = (\sum_{i=1}^{N} h_i)(\sum_{i=1}^{N} h_i/M_i)^{-1} \quad (1)$$

and

$$M_w = (\sum_{i=1}^{N} h_i M_i)(\sum_{i=1}^{N} h_i)^{-1} \quad (2)$$

where h_i and M_i are the height of the HPSEC chromatogram and the molecular weight eluted at volume i (*25*). Our assumption that sample absorptivity is independent of molecular weight may result in an underestimation of M_w and M_n by 5−15% (*12*), but it does not impair identification of chromatogram shifts, which are indicative of fractionation. Repeated measurements on the same sample yield standard deviations for M_w and M_n to be ±200 and ±100, respectively.

Results and Discussion

SHA Transport in Saturated and Unsaturated Sand. Adsorption of SHA to the sand was undetectable at pH 7.3, as the SHA breakthrough curve matched the breakthrough curve of bromide, a nonsorbing tracer (Figure 2A). Rate-limited reactions with the quartz sand exerted a minor influence on SHA transport at pH 5 and pH 3.9 (Figure 2B,C); however, for both treatments, less than 2.5% of the injected SHA mass was retained at quartz interfaces (Table 1). This limited adsorption is attributable to repulsive electrostatic interactions that arise between the negatively charged SHA and quartz−sand surfaces and is consistent with published studies that report nonreactive transport of NOM through quartz media (*17*, *26*).

Breakthrough concentrations of SHA in the unsaturated experiments were consistently lower than those measured in the saturated experiments (Figure 3A−D), indicating that the presence of the air phase enhanced SHA retention within the columns. The mass of SHA retained within the columns varied inversely with pH, ranging from 6.8% at pH 8 to 33.7% at pH 3.9 (Table 1). The breakthrough curves exhibited tailing (Figure 3A−D), which when taken together with the observed slow approach to $C/C_0 = 1$ is indicative of rate-limited desorption.

Effects of pH Changes on SHA Desorption from Air−Water Interfaces. We measured the release of adsorbed SHA from air−water interfaces at the conclusion of the experiment conducted at pH 3.9 by increasing the influent pH to 5 (for 2.3 pore volumes) and then to 7.3 (for 14.3 pore volumes). SHA desorption in response to the initial pH change was small, resulting in only a 0.2 mg/L rise in effluent concentrations (Figure 4). The second pH change promoted substantial release of SHA that coincided with a steep increase in effluent pH from 4.5 to 6.7 (Figure 4). The concentration of SHA briefly peaked at 6.3 mg/L and then slowly declined as the outflow pH gradually climbed toward the influent value of 7.3. Results of mass balance calculations reveal that 50% of the SHA originally adsorbed at pH 3.9 remained bound at the conclusion of the desorption phase. This corresponds to 11% of the injected SHA mass, which is nearly the same as the mass of SHA adsorbed in the unsaturated experiment at pH 7.3 (Table 1).

Analysis of Fractionation during Transport. HPSEC chromatograms for the influent samples (prepared at different pH values) share the same basic features: a single broad peak centered at a molecular weight of 7000, with a prominent shoulder at 2100 Da, and significant tailing at low molecular weights (Figure 5). A second sharp peak occurs at approximately 25 kDa and represents that portion of SHA with a molecular weight that exceeds the high cutoff of the HPSEC column. These large molecules were unable to permeate into the column matrix, so they passed rapidly through the HPSEC column. Polydispersity, M_w, and M_n of the influent samples

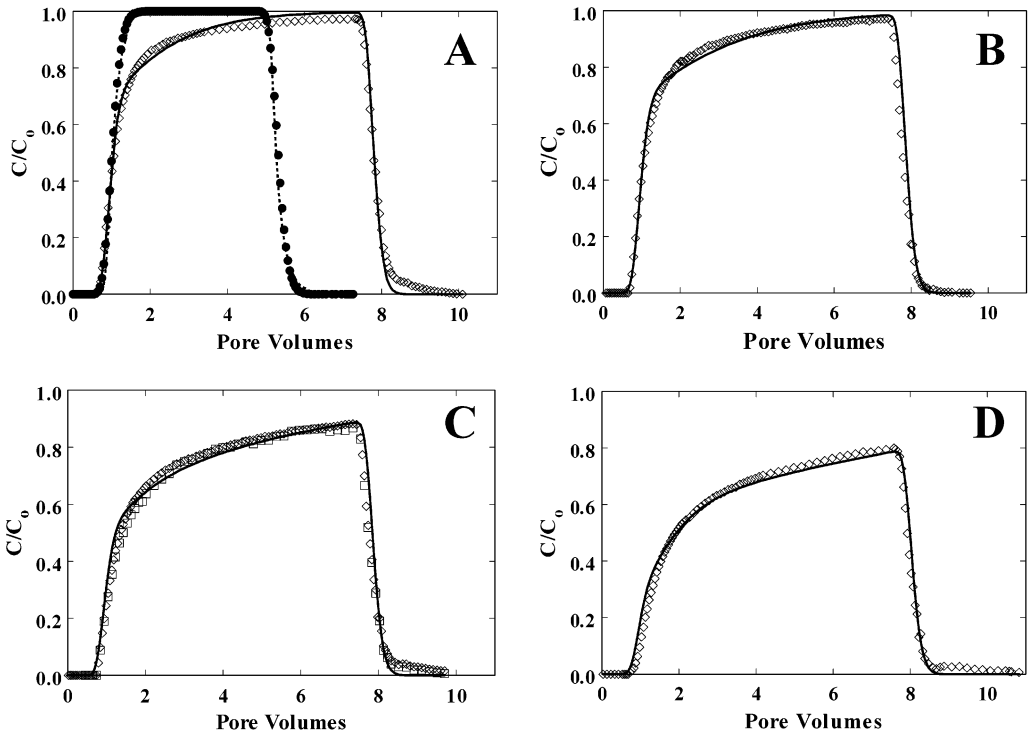

FIGURE 3. Observed SHA breakthrough curves (open diamonds and open squares) for experiments in unsaturated media ($\Theta = 0.12$) at pH (A) 8, (B) 7.3, (C) 5, and (D) 3.9. The solid lines represent breakthrough curves calculated with a model for rate-limited adsorption at solid−and air−water interfaces (see eqs 3−5). The open diamonds represent SHA concentrations measured by the UV−vis spectrophotometer. Breakthrough concentrations measured by the TOC analyzer (open squares) were identical to those measured by the spectrophotometer and hence are only shown in panel C. Measured (solid circles) and modeled (dashed line) bromide breakthrough curves are shown in panel A.

TABLE 1. Summary of Experimental Conditions and Model Results[a]

	unsaturated					saturated				
experimental pH	retained[b] mass (mg)	k_{AW} (h^{-1})	X_{AW} (mg/L)	X_{AW}' [c] (mg/m^2)	R^2	retained[d] mass (mg)	k_{SW} (h^{-1})	X_{SW} (mg/g)	X_{SW}' [c] (mg/m^2)	R^2
3.9	23.6	0.64 (0.02)	39.1 (2.1)	0.93	0.986	3.7	0.85 (0.07)	0.00047 (0.00002)	0.068	0.994
5.0	16.1	0.50 (0.02)	21.0 (1.1)	0.50	0.984	1.9	0.35 (0.06)	0.00028 (0.00003)	0.041	0.994
7.3	8.3	0.43 (0.02)	7.94 (0.37)	0.19	0.991	0	0	0	0	0.997
8.0	4.8	0.44 (0.03)	5.47 (0.41)	0.13	0.988	0	0	0	0	

[a] Standard errors of the parameter estimates are given in parentheses. [b] Total injected mass of SHA for all unsaturated experiments was 70 mg. [c] Calculated from X_{AW} and X_{SW} using an air−water interfacial area (per unit void volume) of 420 cm^{-1} and a sand surface area of 0.0069 m^2/g, which was computed assuming spherical and nonporous grains (*40*). [d] Total injected mass of SHA was 199 mg at pH 3.9 and 79 mg at pH 5.0 and pH 7.3.

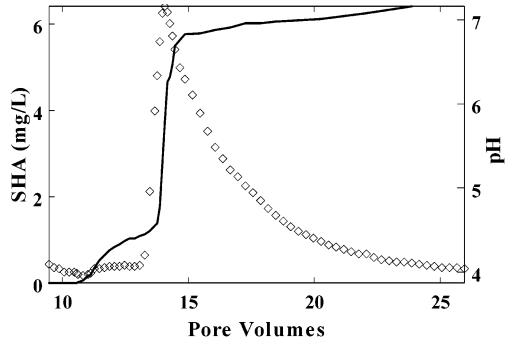

FIGURE 4. Effluent SHA concentrations (open diamonds) and effluent pH (solid line) measured during the desorption phase. The influent pH was increased from 3.9 to 5 at 10.2 pore volumes and from 5 to 7.3 at 12.5 pore volumes.

showed little variation over the pH range tested (Table 2) and are similar in magnitude to values published for other SHAs (*12*, *27*).

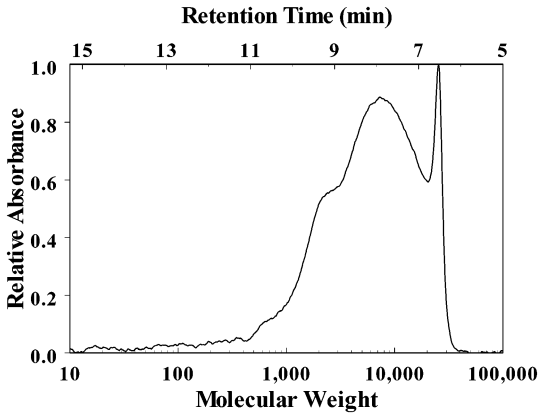

FIGURE 5. Example HPSEC chromatogram for a 20 mg/L solution of SHA.

Adsorptive fractionation involves the selective removal of components of the NOM pool on the basis of molecular

TABLE 2. Molecular Weight Averages and Polydispersity of SHA Injection Solutions

pH	M_w	M_n	polydispersity
3.9	9000	2600	3.5
5.0	9000	2750	3.3
7.2	9050	2750	3.3
8.0	9100	2600	3.5

weight or chemical composition (*28*). For our transport experiments, fractionation by molecular weight is signaled by changes in the HPSEC chromatograms (as quantified by M_w, M_n, and polydispersity) between the influent and effluent samples. Changes in the chemical composition of the NOM pool are reflected by variations in UV absorptivity (i.e., ratio of sample absorbance to carbon concentration); therefore, deviations between breakthrough curves measured with the TOC analyzer and with the spectrophotometer delineate a shift in the sample UV absorptivity and thus fractionation by chemical composition.

In the unsaturated experiments, M_w exhibited a slight shift to lower values at pH 8 and pH 3.9 (Figure 6A,D) but remained unchanged at pH 7.3 and pH 5 (Figure 6B,C). Significant variation in M_n and polydispersity were not detected in any of the unsaturated experiments (Figure 6A−D). In saturated media at pH 3.9, we observed a shift in M_w to slightly higher values during the initial stages of breakthrough (Figure 6E). Nevertheless, M_w for the effluent and influent samples nearly matched after 3.2 pore volumes and changes in the polydispersity and M_n were not apparent. Because SHA adsorption to the saturated media was negligible at pH 5 and pH 7.3, HPSEC analysis was not performed on the effluent samples. Like fractionation by size, fractionation by chemical composition was minimal as breakthrough concentrations of SHA measured by the TOC analyzer matched those determined by UV absorption in both the unsaturated and the saturated experiments (e.g., Figures 2B and 3C).

NOM adsorption is governed by the same specific and electrostatic interactions as polyelectrolyte adsorption, and thus, the adsorptive behavior of polyelectrolytes can provide insight into NOM adsorption reactions and interfacial conformation (*28*−*31*). Polyelectrolyte adsorption at the air−water interface is influenced by strongly attractive nonelectrostatic interactions (e.g., hydrophobic expulsion) between the interface and the segments of the adsorbing molecule (*32*−*34*). These attractive interactions are opposed by mutually repulsive interactions that emanate from the negatively charged molecule segments (*32*, *33*). Electrostatic charges are poorly screened at low ionic strength, and during adsorption each segment is forced to lay flat and in contact with the interface to minimize between-segment repulsive forces (*32*, *33*, *35*). When combined, these interactions promote nonspecificity in the adsorption of polyelectrolyte segments at the air−water interface (*32*, *33*, *35*, *36*). They would also minimize the molecular weight-based selectivity of the air−water interface for various components of the NOM pool, which is consistent with the limited fractionation observed in our column experiments.

Mathematical Model for SHA Adsorption and Transport. We applied a model for coupled transport and mass transfer to the SHA breakthrough-curve data to quantify the kinetics of SHA adsorption under steady porewater flow and pH. Water flow in our unsaturated columns occurred simultaneously through films of water adsorbed to the sand grains, narrow water-filled pores, and interconnected water ducts that lined the corners of partially saturated angular pores (*37*, *40*). On the basis of this conceptualization of air−water configuration, we assume that adsorption of SHA occurs at both air−water and solid (quartz)−water interfaces. The results of the HPSEC and UV analysis suggests that fractionation of SHA during transport through the sand columns was negligible, so we assume that the components of the NOM pool are homogeneous with respect to their adsorption characteristics.

The one-dimensional form of the advection−dispersion equation describes SHA transport through the sand columns:

$$\frac{\partial C}{\partial t} + \frac{\rho_b}{\Theta}\frac{\partial S_{SW}}{\partial t} + \frac{\Theta_A}{\Theta}\frac{\partial S_{AW}}{\partial t} = \frac{qA_L}{\Theta}\frac{\partial^2 C}{\partial z^2} - \frac{q}{\Theta}\frac{\partial C}{\partial z} \qquad (3)$$

where C is the porewater SHA concentration (milligrams of SHA per liter of porewater); t is time (h); ρ_b is the porous-medium bulk density (g L^{-1}); Θ is the volumetric moisture content; S_{SW} is the concentration of SHA adsorbed to the solid−water interfaces (milligrams of SHA per gram of sand); Θ_A is the volumetric air content ($\Theta_A = n - \Theta$, where n equals porosity); S_{AW} is the concentration of SHA adsorbed to the air−water interfaces (milligrams of SHA per liter of air); A_L is the longitudinal dispersivity; z is the coordinate parallel to flow; and q is the specific discharge. Equation 3 is coupled with two rate laws that describe temporal changes in adsorbed concentrations of SHA.

We use second-order rate laws to quantify SHA adsorption. Desorption of adsorbed SHA occurs in our experiments, but inspection of the breakthrough curves suggests that this desorption is small and plays a minor role in SHA transport through the columns. Therefore, we assume that SHA adsorption at air−water and solid−water interfaces can be approximated as irreversible reactions, such that

$$\frac{\rho_b}{\Theta}\frac{\partial S_{SW}}{\partial t} = k_{SW}\left[\frac{X_{SW} - S_{SW}}{X_{SW}}\right]C \qquad (4)$$

and

$$\frac{\Theta_A}{\Theta}\frac{\partial S_{AW}}{\partial t} = k_{AW}\left[\frac{X_{AW} - S_{AW}}{X_{AW}}\right]C \qquad (5)$$

where k_{SW} (h^{-1}) and k_{AW} (h^{-1}) are rate coefficients for SHA adsorption to the solid−water and air−water interface, respectively; X_{SW} is the sorption capacity of the quartz sand (mg g^{-1}); and X_{AW} is the sorption capacity of the air−water interfaces (mg L^{-1}). According to eqs 4 and 5, adsorption rates vary with the product of the porewater SHA concentration and the fraction of unoccupied interface sites. For conditions in which the interface sorption capacity greatly exceeds the adsorbed concentration (e.g., $X_{AW} \gg S_{AW}$), eqs 4 and 5 reduce to first-order reactions whereby the adsorption rate varies linearly with C. Equations 3−5 were solved numerically using a finite-difference method with a predictor−corrector time-stepping scheme. We assumed a specified SHA concentration at the column surface, a zero gradient in porewater SHA concentrations at the column base, and zero initial adsorbed and aqueous concentrations of SHA.

SHA Adsorption Kinetics in Unsaturated Media. We ran the model in inverse mode to quantify the influence of pH on the kinetics of SHA adsorption to the air−water interfaces. The parameters that govern air−water interface reactions were estimated from the breakthrough data on SHA transport through unsaturated media using a Levenberg−Marquardt least-squares algorithm. The remaining model parameters, that is, those governing dispersion (A_L) and SHA adsorption to sand (k_{SW} and X_{SW}), were determined independently from separate experiments. We determined the value of A_L (0.092 cm) from analysis of data on bromide transport through the unsaturated sand. Estimates of k_{SW} and X_{SW} were taken from results of inverse analyses of the breakthrough data measured

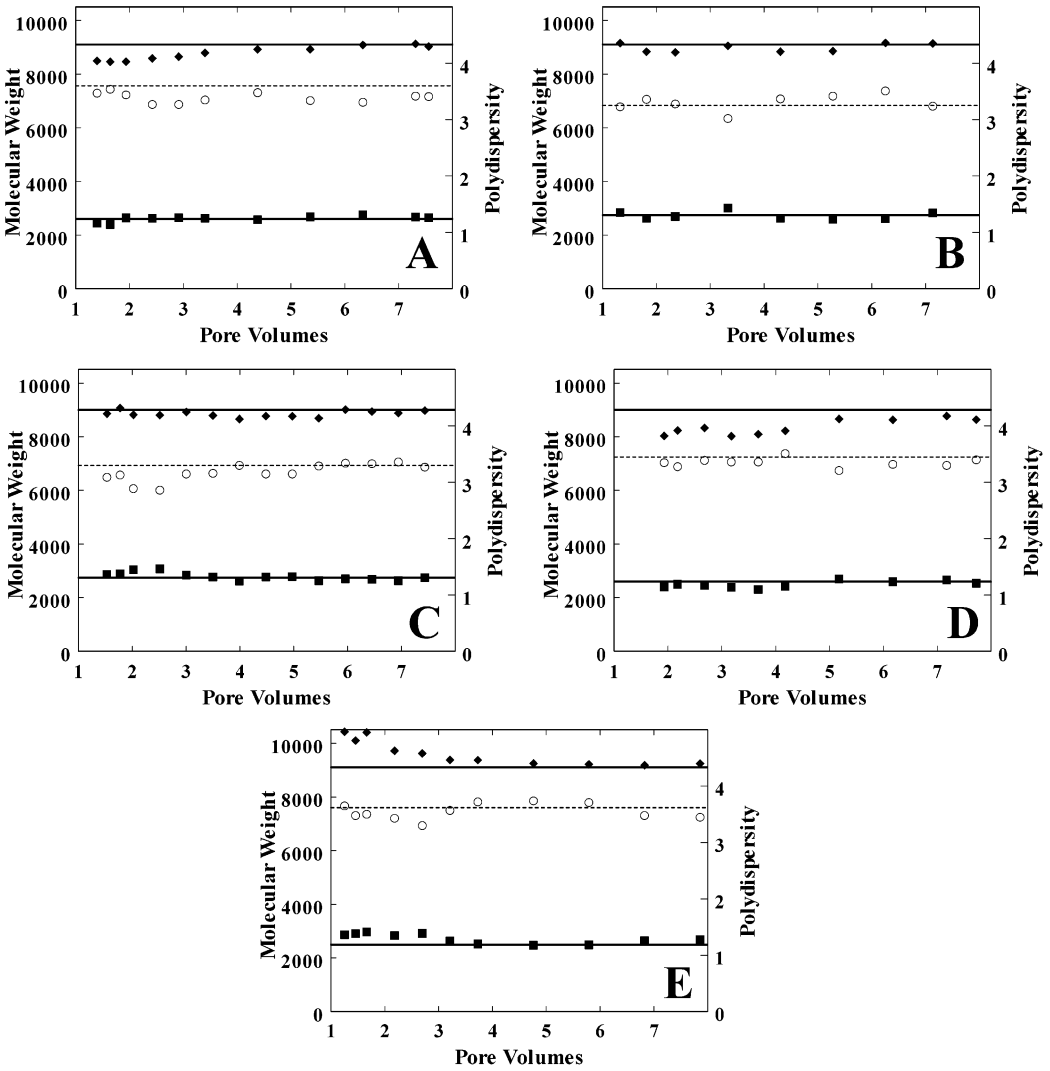

FIGURE 6. M_w **(closed diamonds),** M_n **(closed squares), and polydispersity (open circles) for effluent samples collected in unsaturated experiments at pH (A) 8, (B) 7.3, (C) 5, (D) 3.9, and (E) in the saturated experiment at pH 3.9. The solid and dashed lines represent influent values for the molecular weight averages and polydispersity, respectively.**

in the saturated experiments. (See Figure 2 for model fits and Table 1 for best-fit values of k_{SW} and X_{SW}.) Adsorption to the sand was small for all treatments but undetectable in the saturated experiments at pH 7.3 and pH 8, such that transport in these cases could be simulated with $k_{SW} = X_{SW} = 0$.

The calculated breakthrough curves match the data closely (R^2 values in Table 1; Figure 3), indicating that a model incorporating second-order kinetics expressions for adsorption at the air−water and sand−water interfaces is capable of describing the transport of SHA in unsaturated porous media. The model underestimates concentrations of SHA measured near the end of the experiments because it does not account for desorption (Figure 3). These model data discrepancies are small, however. That is, the model-calculated masses of SHA eluted from the columns (assuming irreversible adsorption) differ from the measured masses of SHA eluted from the column by less than 2.5%, suggesting that our treatment of SHA adsorption as an irreversible mass-transfer process is a good approximation.

Best-fit values of X_{AW} vary linearly with pH, increasing by a factor of 7 as the pH decreases from 8 to 3.9. Once adsorbed at the interface, the negative charge emanating from the dissociated functional groups of each molecule repels approaching SHA molecules. This repulsion between interface-associated and aqueous-phase SHA may limit further adsorption (*38*) in a manner analogous to "blocking" observed during colloid deposition (e.g., ref *39*). We cannot exclude the possibility that other mechanisms, in addition to blocking, affect the SHA adsorption capacity of the air−water interfaces; however, we believe that the inverse relationship between X_{AW} and pH can be attributed, at least in part, to increases in blocking efficiency that occur as the electrostatic charge density of SHA increases with pH.

We normalized the sorption capacities of the air−water and sand−water interfaces (X_{AW} and X_{SW}) to surface area using interfacial areas estimated by Saiers and Lenhart (*40*) for an identical porous medium at $\Theta = 0.12$ (see X_{AW}' and X_{SW}', Table 1). The solid−water and air−water surface area estimates were obtained by applying a liquid−vapor configuration model (*41*) to moisture characteristic data for our quartz sand. Values of X_{AW}' and X_{SW}' decrease linearly with pH from 0.93 to 0.13 mg m^{-2} and from 0.068 to 0.0 mg m^{-2}, respectively. While published values are not available for either quartz−water or air−water interfaces, the adsorption capacity of metal oxide surfaces ranges from 1.5 to 0.2 mg m^{-2}, with the larger values associated with positively charged surfaces (*9, 28, 31, 38, 42*). These results suggest that the affinity of the air−water interface for NOM is strong, comparable to that for positively charged mineral surfaces, and at least an order of magnitude higher than that for negatively charged mineral surfaces.

We find that best-fit values of k_{AW} (the coefficient for the initial adsorption rate of SHA onto bare air−water interfaces) decline from 0.64 h^{-1} at pH 3.9 to 0.44 h^{-1} at pH 8 (Table 1). This trend is qualitatively consistent with our observations for SHA adsorption to the sand−water interfaces (k_{SW}, Table 1) and with published reports for NOM adsorption onto a variety of solid surfaces (*28*, *43*, *44*). The magnitude of k_{AW} depends on the rate at which SHA is transported from the bulk solution to the interface as well as on the strength of the electrostatic and specific interactions that control adsorption. According to Avena et al. (*43*, *45*), changes in the transport rate attributed to expansion or contraction of NOM molecules with pH is negligible. Therefore, variation in k_{AW} reflects pH-induced alteration of the surface adsorption reaction and presumably indicates that the hydrophobic characteristics of SHA vary inversely with pH. Increases in solution pH promotes dissociation of acidic functional groups, leading to larger and more highly charged SHA molecules that prefer the fully solvated aqueous environment to the air−water interface.

In conclusion, we find that mass-transfer reactions with the air phase measurably reduce porewater SHA concentrations during transport through unsaturated media and that the intensity of this mass-transfer reaction is sensitive to porewater pH. Comparisons of our results with those published on NOM adsorption to geologic materials (e.g., refs *28* and *31*) reveal that the retention of NOM at air−water interfaces may be of comparable importance to the retention of NOM at mineral surfaces. Consequently, mass-transfer reactions with the air phase must be included in mathematical models for accurate prediction of the fluxes of NOM and NOM-bound contaminants in the vadose zone. While SHA is polydisperse, significant fractionation in the column experiments did not occur. We cannot rule out the possibility that SHA exhibits a distribution in sorptive affinities for air−water interfaces under equilibrium conditions, but in our column experiments, as in natural vadose zone settings during infiltration events, transport time scales are too short to permit establishment of equilibrium. Our results, then, suggest the adsorption *rates*, but not necessarily equilibrium-partitioning affinities, are approximately constant for all components of the SHA pool. Though SHA adsorption could be closely approximated as an irreversible mass-transfer process, desorption of SHA was detectable, even under steady chemical conditions. This slow desorption would not significantly affect porewater concentrations of NOM on the time scale of typical infiltration events, but it could influence the fate of NOM within the vadose zone over longer time scales of days or weeks.

Acknowledgments

This research was supported by the Hydrological Sciences Program of the National Science Foundation through Grant EAR-990958. Three anonymous reviewers provided thoughtful recommendations for revision that improved the manuscript.

Literature Cited

(1) McCarthy, J. F.; Zachara, J. M. *Environ. Sci. Technol.* **1989**, *23*, 496−502.
(2) Chen, Y.; Schnitzer, M. *Soil Sci.* **1978**, *125*, 7−15.
(3) Hayase, K.; Tsubota, H. *J. Colloid Interface Sci.* **1986**, *114*, 220−226.
(4) Schnitzer, M.; Khan, S. U. *Humic Substances in the Environment*; Marcel Dekker: New York, 1972.
(5) Thurman, E. M. *Organic Geochemistry of Natural Waters*; Martinus Nijhoff/Dr W. Junk Publishers: Boston, 1985.
(6) Sposito, G. *The Chemistry of Soils*; Oxford University Press: New York, 1989.
(7) Drever, J. I. *The Geochemistry of Natural Waters*, 2nd ed.; Prentice Hall: Englewood Cliffs, NJ, 1988.
(8) Davis, J. A. *Geochim. Cosmochim. Acta* **1982**, *46*, 2381−2393.
(9) Schlautman, M. A.; Morgan, J. J. *Geochim. Cosmochim. Acta* **1994**, *58*, 4293−4303.
(10) Anderson, M. A.; Hung, A. Y. C.; Mills, D.; Scott, M. S. *Soil Sci.* **1995**, *160*, 111−116.
(11) Meier, M.; Namjesnik-Dejanovic, K.; Maurice, P. A.; Chin, Y.-P.; Aiken, G. R. *Chem. Geol.* **1999**, *157*, 275−284.
(12) Kilduff, J. E.; Karanfil, T.; Chin, Y.-P.; Walter, J. Weber, J. *Environ. Sci. Technol.* **1996**, *30*, 1336−1343.
(13) Davis, J. A.; Gloor, R. *Environ. Sci. Technol.* **1981**, *15*, 1223−1229.
(14) Gu, B.; Schmitt, J.; Chen, Z.; Liang, L.; McCarthy, J. F. *Geochim. Cosmochim. Acta* **1995**, *59*, 219−229.
(15) Johnson, W. P.; Bao, G.; John, W. W. *Environ. Sci. Technol.* **2002**, *36*, 608−616.
(16) McCarthy, J. F.; Williams, T. M.; Liang, L.; Jardine, P. M.; Jolley, L. W.; Taylor, D. L.; Palumbo, A. V.; Cooper, L. W. *Environ. Sci. Technol.* **1993**, *27*, 667−676.
(17) Weigand, H.; Totsche, K. U. *Soil Sci. Soc. Am. J.* **1998**, *62*, 1268−1274.
(18) Dunnivant, F. M.; Jardine, P. M.; Taylor, D. L.; McCarthy, J. F. *Soil Sci. Soc. Am. J.* **1992**, *56*, 437−444.
(19) Jardine, P. M.; Dunnivant, F. M.; Selim, H. M.; McCarthy, J. F. *Soil Sci. Soc. Am. J.* **1992**, *56*, 393−401.
(20) Lenhart, J. J.; Saiers, J. E. *Environ. Sci. Technol.* **2002**, *36*, 769−777.
(21) Chen, Y.; Senesi, N.; Schnitzer, M. *Soil Sci. Soc. Am. J.* **1977**, *41*, 352−358.
(22) Traina, S. J.; Novak, J.; Smeck, N. E. *J. Environ. Qual.* **1990**, *19*, 151−153.
(23) Chin, Y.-P.; Aiken, G.; O'Loughlin, E. *Environ. Sci. Technol.* **1994**, *28*, 1853−1858.
(24) Zhou, Q.; Cabaniss, S. E.; Maurice, P. A. *Water Res.* **2000**, *34*, 3505−3414.
(25) Yau, W.; Kirkland, J. J.; Bly, J. J. *Modern Size Exclusion Chromatography*; Wiley: New York, 1979.
(26) Liu, H.; Amy, G. *Environ. Sci. Technol.* **1993**, *27*, 1553−1562.
(27) Beckett, R.; Jue, Z.; Giddings, J. C. *Environ. Sci. Technol.* **1987**, *21*, 289−295.
(28) Zhou, Q.; Maurice, P. A.; Cabaniss, S. E. *Geochim. Cosmoch. Acta* **2001**, *65*, 803−812.
(29) Vermeer, A. W. P.; Koopal, L. K. *Langmuir* **1998**, *14*, 4210−4216.
(30) Tiller, C. L.; O'Melia, C. R. *Colloids Surf. A* **1993**, *73*, 89−102.
(31) Au, K.-K.; Penisson, A. C.; Yang, S.; O'Melia, C. R. *Geochem. Cosmochim. Acta* **1999**, *63*, 2903−2917.
(32) Yim, H.; Kent, M.; Matheson, A.; Ivkov, R.; Satija, S.; Majewski, J.; Smith, G. S. *Macromolecules* **2000**, *33*, 6126−6133.
(33) Van der Schee, H. A.; Lyklema, J. *J. Phys. Chem.* **1984**, *88*, 6661−6667.
(34) Papenhuijzen, J.; Schee, H. A. v. d.; Fleer, G. J. *J. Colloid Interface Sci.* **1985**, *104*, 540−552.
(35) Scheutjens, J. M. H. M.; Fleer, G. J. *J. Phys. Chem.* **1980**, *84*, 178−190.
(36) van de Steeg, H. G. M.; Cohen Stuart, M. A.; de Keizer, A.; Bijsterbosch, B. H. *Langmuir* **1992**, *8*, 2538−2546.
(37) Tuller, M.; Or, D. *Water Resour. Res.* **2001**, *37*, 1257−1276.
(38) Vermeer, A. W. P.; van Riemsdijk, W. H.; Koopal, L. K. *Langmuir* **1998**, *14*, 2810−2819.
(39) Song, L.; Elimelech, M. *Colloids Surf. A* **1993**, *73*, 49−63.
(40) Saiers, J. E.; Lenhart, J. J. *Water Resour. Res.* **2003**, *39* (9), 1256; doi: 10.1029/2002WR001887.
(41) Tuller, M.; Or, D.; Dudley, L. M. *Water Resour. Res.* **1999**, *35*, 1949−1964.
(42) Wang, L.; Chin, Y.-P.; Traina, S. J. *Geochim. Cosmochim. Acta* **1997**, *61*, 5313−5324.
(43) Avena, M. J.; Koopal, L. K. *Environ. Sci. Technol.* **1999**, *33*, 2739−2744.
(44) Jones, K. L.; O'Melia, C. R. *J. Membr. Sci.* **2000**, *165*, 31−46.
(45) Avena, M. J.; Vermeer, A. W. P.; Koopal, L. K. *Colloids Surf. A* **1999**, *151*, 213−224.

Received for review April 29, 2003. Revised manuscript received September 30, 2003. Accepted October 6, 2003.

ES034409A